arXiv:cond-mat/0405355v1 [cond-mat.soft] 17 May 2004

Two-dimensional loosely and tightly bound solitons in optical lattices and inverted traps

H Sakaguchi† and B A Malomed‡
† Department of Applied Science for Electronics and Materials,
Interdisciplinary Graduate School of Engineering Sciences,
Kyushu University, Kasuga, Fukuoka 816-8580, Japan
‡ Department of Interdisciplinary Studies,Faculty of Engineering,
Tel Aviv University, Tel Aviv 69978, Israel

February 2, 2008

Abstract

We study the dynamics of nonlinear localized excitations ("solitons") in two-dimensional (2D) Bose-Einstein condensates (BECs) with repulsive interactions, loaded into an optical lattice (OL), which is combined with an external parabolic potential. First, we demonstrate analytically that a broad ("loosely bound", LB) soliton state, based on a 2D Bloch function near the edge of the Brillouin zone (BZ), has a negative effective mass (while the mass of a localized state is positive near the BZ center). The negative-mass soliton cannot be held by the usual trap, but it is safely confined by an inverted parabolic potential (*anti-trap*). Direct simulations demonstrate that the LB solitons (including the ones with intrinsic vorticity) are stable and can freely move on top of the OL. The frequency of elliptic motion of the LB-soliton's center in the anti-trapping potential is very close to the analytical prediction which treats the solition as a quasi-particle. In addition, the LB soliton of the vortex type features real rotation around its center. We also find an abrupt transition, which occurs with the increase of the number of atoms, from the negative-mass LB states to tightly bound (TB) solitons. An estimate demonstrates that, for the zero-vorticity states, the transition occurs when the number of

atoms attains a critical number $N_{\rm cr} \sim 10^3$, while for the vortex the transition takes place at $N_{\rm cr} \sim 5 \cdot 10^3$ atoms. The positive-mass LB states constructed near the BZ center (including vortices) can move freely too. The effects predicted for BECs also apply to optical spatial solitons in bulk photonic crystals.

1 Introduction

Periodic potentials, usually called optical lattices (OL), which are induced by interference of laser beams illuminating a Bose-Einstein condensate (BEC), are widely used in experimental studies of BECs. Not only one-dimensional (1D) OLs, but also their multidimensional counterparts are available in the experiment, see Refs. [1] and references therein.

An important type of nonlinear excitations that BECs may support are bright solitons (in this paper, following the trend commonly adopted in the current literature, we apply the term "soliton" to robust localized objects, without implying integrability of the underlying mathematical model). In an effectively 1D ("cigar-shaped") condensate, solitons have been observed in the experiment [2]. Creation of solitons in a BEC confined in the OL has not been reported yet, although splitting of wave packets in a ^{87}Rb condensate, loaded in a cylindrical trap with an superimposed 1D OL potential, which was reported recently [3], might be a manifestation of transient soliton dynamics.

Parallel to the experiments, many theoretical predictions for BEC solitons in OLs have been reported. In particular, attention was attracted to a possibility to create *gap solitons*, that are expected as a result of the interplay of the OL potential and *repulsive* interaction between atoms in the BEC [4, 5]. While only 1D solitons have been thus far observed in BECs, it was predicted that OLs may support multidimensional solitons of the gap type as well [4]. A prediction which is especially relevant to feasible experiments is that OLs can also stabilize multidimensional solitons in BECs with attraction between atoms (because of the possibility of collapse, such solitons are unstable without a support potential) [6]. Moreover, 2D bright solitons carrying intrinsic vorticity can be stabilized too by the OL in the 2D case [6, 7]. Various other properties of OL-supported solitons were studied too [8].

Similar localized objects are expected in a different physical setting, in the form of 2D optical spatial solitons in nonlinear photonic crystals (NPCs)

[9, 6, 7]. In optical media, an effective lattice potential is induced by periodic modulation of the local refractive index in the transverse direction(s) [10, 6, 7]. An alternative is to use a *virtual lattice*, induced in a photorefractive medium by a transverse array of strong coherent laser beams; the latter arrangement has made it possible to observe 2D spatial solitons in a real experiment [11], as well as their vorticity-carrying counterparts [12] .

Most theoretical studies of solitons in the above-mentioned models did not address their motion. In a recent work [13], we considered in detail the motion and collisions of 1D solitons in the OL-equipped model in both cases of the attractive and repulsive cubic nonlinearity. In that work, the OL potential was combined with an external parabolic (harmonic) trapping potential, which corresponds to the real situation in any BEC experiment. Direct simulations of the corresponding effective 1D Gross-Pitaevskii (GP) equation had demonstrated that, in either case (self-focusing or self-defocusing nonlinearity), the soliton travels freely through the lattice if its norm (number of atoms) is below a certain critical value; above this value, it gets trapped by the OL. Depending on parameters, collisions between moving solitons are either elastic, or lead to their fusion. The most intriguing result concerns the motion of the soliton in the parabolic trap: in the case of attraction, the soliton behaves, as it may be naturally expected, as a quasi-particle in the harmonic-oscillator potential. However, in the case of repulsion, the soliton of the gap type is expelled by the parabolic trap, while it is stably confined by an *anti-trap* (repulsive parabolic potential). This result, which calls for direct experimental verification, was supported by analytical considerations which demonstrate that the effective mass of the gap soliton, regarded as a quasi-particle, is *negative* (in the case of the usual soliton, corresponding to the attractive nonlinearity, the effective mass is positive).

An issue of straightforward interest is to extend these results to the 2D case, which is quite relevant, as experiments with 2D solitons in BECs seem possible right now. Besides that, the problem is also of direct relevance for steering spatial optical soliton in NPC media. In this work, we focus on the 2D BEC model with repulsive interactions, as this case is most relevant to the experiment, and produces most interesting physical results. First, we demonstrate that broad localized states, which we call loosely bound (LB) ones, may be represented as a product of a linear Bloch function, defined by the OL, which is taken close to the edge to the corresponding Brillouin zone (BZ), and a slowly varying envelope function, which obeys an asymptotic nonlinear equation that does not contain OL. Such a representation makes

it possible to demonstrate analytically that the effective mass of the LB state is negative. This way, we find not only fundamental LB states, but also ones carrying vorticity, whose mass is negative too; the existence of 2D localized vortices in the repulsive model has not been reported before. In direct simulations, the LB vortex features actual rotation around its center. Simulations confirm the stability of the localized LB states, and demonstrate that they can move freely through the OL. In particular, both fundamental and vortex LB states can be readily set in elliptic circular motion in the anti-trapping potential, the frequency of the circulations being very accurately predicted by the asymptotic equation.

Direct simulations (as well as the asymptotic equation) demonstrate an abrupt transition (without hysteresis) from the LB states to much stronger localized tight-bound (TB) ones with the increase of the norm (number of atoms). The TB states are nothing else but the 2D gap solitons, that were first found in Ref. [4]. The LB-TB transition also takes place for the vortices, thus revealing the existence of new TB vortex solitons of the gap type. It is additionally found that the TB vortices undergo an intrinsic transition to a more symmetric shape with subsequent increase of the norm. Unlike their LB counterparts, the TB solitons cannot move, being strongly pinned by the OL.

We also construct LB states, starting from the linear Bloch function close to the BZ center. In that case, the effective mass is positive, no transition to TB solitons occurs (as they do not exist), and the LB states, both fundamental and vortex ones, are mobile, which is accurately described by the corresponding asymptotic equation.

The rest of the paper is organized as follows. The analysis based on the derivation of the asymptotic equations for the LB states, with both negative and positive mass, is presented in section 2. Numerical results for static solitons (however, including rotation of the vortex LB states), such as the LB-TB transitions, are summarized in section 3. In section 4, we present numerical and analytical results concerning motion of the LB states, for the cases of the negative and positive mass. The paper is concluded by section 5.

2 Formulation of the model and the analytical approximation

2.1 The Gross-Pitaevskii equations

The mean-field description of the BEC dynamics is based on the GP equation for the mean-field wave function ψ in three dimensions [14],

$$i\hbar\frac{\partial\psi}{\partial t}=\left[-\frac{\hbar^2}{2m}\nabla^2+U\left(\mathbf{r}\right)+G|\psi|^2\right]\psi, \tag{1}$$

where m is the atomic mass, $G\equiv 4\pi\hbar^2 a/m$, a is the s -wave scattering length, U is the potential applied to the condensate, and the number of atoms is $\int|\psi|^2 d\mathbf{r}$. As is well known [4, 5, 15], in the case of a pancake-shaped configuration (when the frequency characterizing the confining potential in the transverse direction is much larger than the confining frequencies corresponding to the perpendicular directions), Eq. (1) can be reduced to a 2D equation. After appropriate rescalings, such as $t'=\hbar t/(m\lambda^2), x'=x/\lambda, y'=y/\lambda$ and $\phi=G^{1/2}\psi$, where λ is the period of the spatially periodic potential, it takes the form

$$i\phi_t=-\frac{1}{2}\nabla^2\phi+\left\{|\phi|^2-\varepsilon\left[\cos(2\pi x)+\cos(2\pi y)\right]+\frac{1}{2}B(x^2+y^2)\right\}\phi, \tag{2}$$

where ϕ is the renormalized wave function, the sign $'$ denoting the rescaled coordinates x', y', t' is omitted, the kinetic-energy operator ∇^2 acts on the coordinates x and y, the repulsive interaction between atoms is assumed, the OL period is normalized to be 1 in both directions (we consider the simplest case of the square lattice, although more sophisticated patterns, such as triangular, hexagonal, and quasi-periodic ones, may be interesting too), while ε and B are amplitudes of the, respectively, OL and parabolic potential (in simulations, we will fix $\varepsilon=10$ and $B=-0.005$, or $\varepsilon=5$ and $B=+0.005$, negative B implying the anti-trapping potential). We will show the numerical results with the dimensionless equation (2). The unit length corresponds to the spatial period λ of the optical lattice, and the unit time corresponds to $m\lambda^2/\hbar\sim 1.3\times 10^{-3}$s for $\lambda\sim 10^{-6}$m and $m(^{87}\mathrm{Rb})\sim 1.37\times 10^{-25}$kg.

If $B=0$ and the nonlinear term is neglected, Eq. (2) becomes the ordinary 2D linear Schrödinger equation with the periodic potential, which has Bloch-state solutions. The Bloch function $F(x,y)$ obeys the equation

$$\mu F(x,y)=\frac{1}{2}\nabla^2 F+\varepsilon\left[\cos(2\pi x)+\cos(2\pi y)\right]F, \tag{3}$$

where μ is the chemical potential (or simply energy, in the case of a single atom), and the solution is quasi-periodic, i.e., $F(x,y) = \exp\left(ik_x x + ik_y y\right)\ f(x,y)$, where $k_{x,y}$ are two wavenumbers, and the function $f(x,y)$ is periodic, such that $f(x+1,y) = f(x,y), f(x,y+1) = f(x,y)$. The Bloch-wave solution determines the energy-band structure, $\mu = \mu(k_x, k_y)$, the point $(k_x, k_y) = (\pi, \pi)$ being the edge of the BZ (Brillouin zone).

Following the lines of the analytical approach to the 1D case developed in Ref. [13], an approximate solution to the full time-dependent GP equation (2) for a small-amplitude broad localized state ("soliton") may be sought for, in the lowest approximation, as

$$\phi(x,y,t) = e^{-i\mu t} F(x,y)\Phi(x,y,t), \tag{4}$$

where $F(x,y)$ is the Bloch function defined above, and $\Phi(x,y,t)$ is an envelope function which varies slowly (as a function of x and y) in comparison with $F(x,y)$. This ansatz actually assumes that the nonlinearity and parabolic potential in Eq. (2) are small perturbations in comparison with the OL terms. The most typical gap soliton corresponds to a solution which approaches the linear Bloch function with $k_x = k_y = \pi$ when its norm (the number of atoms), $N \equiv \int_{-\infty}^{+\infty} |\phi|^2 dxdy$, tends to zero (cf. a similar situation in the 1D case [13]).

In the general case, the slowly varying amplitude Φ obeys an asymptotic NLS equation, that can be derived by substituting the ansatz (4) into Eq. (2) and applying a known averaging procedure [4]:

$$i\frac{\partial \Phi}{\partial t} = -\frac{1}{2} M_{\rm eff}^{-1} \nabla^2 \Phi + g|\Phi|^2 \Phi + \frac{1}{2} B(x^2+y^2)\Phi. \tag{5}$$

Here, the effective mass $M_{\rm eff}$ for linear excitations is determined from the curvature of the energy-band structure of the linear Bloch states, $M_{\rm eff}^{-1} = (1/2)\left(\partial^2/\partial k_x^2 + \partial^2/\partial k_y^2\right)\mu$, and

$$g \equiv \frac{\int_0^1 \int_0^1 |F(x,y)|^4 dxdy}{\int_0^1 \int_0^1 |F(x,y)|^2 dxdy}\ . \tag{6}$$

The energy functional corresponding to the simplified GP equation (5) is

$$E = \frac{1}{2}\int\int dxdy \left[M_{\rm eff}^{-1} |\nabla\Phi|^2 + g\,|\Phi|^4 + B\left(x^2+y^2\right)|\Phi|^2\right]. \tag{7}$$

Stationary solutions to the asymptotic equation (5) can be looked for in an obvious form,

$$\Phi = f(r) \exp\left[i\left(m\theta - \mu t\right)\right], \tag{8}$$

where r and θ are polar coordinates in the plane (x, y), $m = 0, 1, 2, ...$ is a possible vorticity of the solution, and the amplitude $f(r)$ obeys an equation

$$f'' + r^{-1} f' - m^2 r^{-2} = -2M_{\text{eff}} \left[\mu - (B/2)\, r^2 - g f^2\right] f \tag{9}$$

[in the general case – in particular, in the case of the full GP equation (2) which is not isotropic – the vorticity of a stationary solution may be defined as $\Delta\theta/\left(2\pi\right)$, where $\Delta\theta$ is the total change of the solution's phase along a closed path around the center]. The linear limit of Eq. (9) is the linear Schrödinger equation for the 2D harmonic oscillator. For fixed integer m, the ground-state solution to the latter equation is (in the present notation)

$$f(r) = r^m \exp(-\alpha^2 r^2/2),$$

where $\alpha^2 = \sqrt{BM_{\text{eff}}}$, with $\mu = (m+1)\omega$, and $\omega = \sqrt{B/M_{\text{eff}}}$.

2.2 Solutions near the edge and center of the Brillouin zone

Near the BZ edge, i.e., close to the point $(k_x, k_y) = (\pi, \pi)$, the linear Bloch function can be approximated by a combination of four harmonics:

$$F(x, y) = c_1 \exp(ik_x x + ik_y y) + c_2 \exp\left(i(k_x - 2\pi)x + ik_y y\right)$$

$$+ c_3 \exp\left(ik_x x + i(k_y - 2\pi)y\right) + c_4 \exp\left(i(k_x - 2\pi)x + i(k_y - 2\pi)y\right). \tag{10}$$

The substitution of this into Eq. (3) and a usual truncation procedure (neglecting higher-order spatial harmonics) lead to an expression $\mu(k_x, k_y) = \mu_0^{(\text{edge})} + \left[(k_x - \pi)^2 + (k_y - \pi)^2\right]/(2M_{\text{eff}}^{(\text{edge})})$, where

$$\mu_0^{(\text{edge})} = (\pi^2 \pm |\varepsilon|)/2, \tag{11}$$

$$M_{\text{eff}}^{(\text{edge})} = -\frac{|\varepsilon|}{2\pi^2 - |\varepsilon|} \tag{12}$$

and $g = (3/4)^2$ [recall g is defined by Eq. (6)]; the signs $\pm$ in Eq. (11) pertain to two Bloch-wave solutions which differ by a phase shift relative to

the periodic OL potential in Eq. (3). As is seen, the effective mass in Eq. (12) is negative for the linear excitations near the BZ edge (unless $|\varepsilon|$ is very large, in which case the above approximation does not apply).

Equation (5) with $M_{\text{eff}} < 0$, $g > 0$, and $B < 0$ (anti-trap) is tantamount to the usual 2D GP equation with positive mass, negative g (which corresponds to self-attraction), and $B > 0$ (usual trap, rather than anti-trap). As is well known [16, 17], the GP equation in the latter form has localized solutions, unless the norm N is too large (otherwise, collapse will take place). These solutions, and their comparison with numerically found solutions to the full underlying equation (2), will be displayed below.

An approximation similar to that based on Eq. (10) can also be developed close to the BZ center. At the BZ center, the linear Bloch function may be approximated by

$$F(x, y) = [1 + c_2 \cos(2\pi x)][1 + c_2 \cos(2\pi y)], \tag{13}$$

and the eventual expressions for the effective mass and μ_0 are

$$M_{\text{eff}}^{(\text{center})} = \frac{2\pi^4 + \varepsilon^2 + \pi^2\sqrt{4\pi^4 + 2\varepsilon^2}}{10\pi^4 + \varepsilon^2 - 3\pi^2\sqrt{4\pi^4 + 2\varepsilon^2}} \ , \tag{14}$$

$$\mu_0^{(\text{center})} = \pi^2 - \sqrt{\pi^4 + \varepsilon^2/2}. \tag{15}$$

Other coefficients are found to be $c_2 = -\mu_0/\varepsilon$ and $g = (1 + 12c_2^2 + 6c_2^4)/(1 + 2c_2^2)$. In this case, the effective mass is always positive [in particular, in the case with $\varepsilon = 5$ and $B = 0.005$, for which this approximation will be compared to numerical results below, $M_{\text{eff}}^{(\text{center})} \approx 1.12$]. Obviously, Eq. (9) with $M_{\text{eff}} > 0$, $g > 0$, and $B > 0$ has a localized solution (actually, of the Thomas-Fermi type, see below) for any vorticity m and norm N.

3 Numerical results

3.1 Loosely bound states

Our first objective is to find LB ("loosely bound") localized states near the BZ edge, which can be constructed using the asymptotic GP equation (5) and the relations (4) and (10), and compare them with the corresponding numerical solutions to the full equation (2). The 2D localized solutions to the asymptotic GP equation (5) were found numerically [16, 18], and in an

approximate form they can be also solved by dint of a variational method [17]. In particular, the radial equation (9) can be solved numerically by the shooting method, which simultaneously makes it possible to find the nonlinear eigenvalue μ. Figure 1 displays numerical solutions to Eq. (9) for $m = 0, 1$ and 2, obtained by means of the shooting method. The norm of the corresponding solutions for the underlying wave function ϕ is, according to Eq. (4), $N \approx \int\int f^2(r)\cos^2(\pi x)\cos^2(\pi y)dxdy \approx N_0/4$, where N_0 is the norm of Φ [see Eq. (8)]. In particular, $N = 1.52$ for $m = 0$, $N = 2.98$ for $m = 1$, and $N = 4.08$ for $m = 2$.

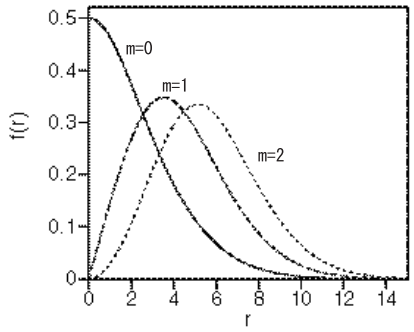

Figure 1: Typical examples of numerically found solutions to Eq. (9) with $M_{\rm eff} = -10/(2\pi^2 - 10), g = (3/4)^2$ and $B = -0.005$ which represent 2D solitons with vorticity $m = 0, 1$ and 2.

To characterize families of the solutions, Figs. 2(a) and 2(b) display, respectively, the absolute value of the energy-per-atom, $-\epsilon = -E/N$ for the solution [the energy E is given by the functional (7)], and the maximum value of $f(r)$ vs. the norm N. In particular, $-\epsilon$ decreases with N, because a larger atom density gives rise a larger positive contribution to E through the term $g|\Phi|^4$ in the energy density. The maximum value of $f(r)$ increases with N, since the effective interaction is attractive owing to the negativeness of $M_{\rm eff}$.

Figures 3(a), (b) and (c) present comparison of the above semi-analytical solutions (for $m = 0, 1$ and 2), based on Eqs. (4), (10) and (5), with direct numerical solutions of the full 2D equation (2). The comparison is performed by displaying the semi-analytical and direct numerical solutions for $|\phi(x, L/2)|$, taken along the central cross-section, at $y = L/2$ (the norms

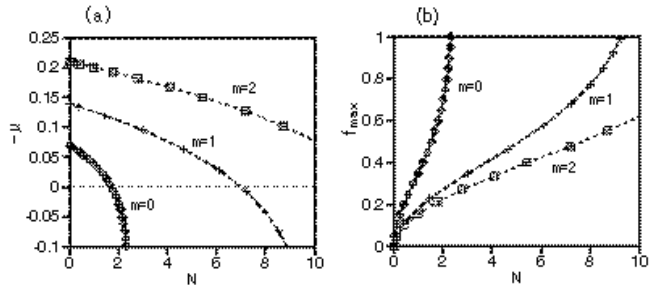

Figure 2: The absolute value of the energy-per-atom, $-\epsilon$, (a) and amplitude (b) of the 2D solitons with the vorticity $0, 1$ and 2, as found from Eq. (9), vs. the norm.

of the numerical and semi-analytical solutions are virtually identical in each case). Fairly good agreement is seen for $m = 0, 1$ and 2, although $|\phi|$ in the direct numerical solutions is slightly larger.

From the viewpoint of the reduced GP equation (5), which does not explicitly contain the OL potential, the angular velocity $\Omega = \mu/m$, which appears in the expression (8), is only a phase velocity. However, the relation (4) suggests that the corresponding solution to the full GP equation (2) may feature *actual rotation* of the pattern with the angular velocity Ω. Direct simulations confirm this expectation, as shown in Fig. 4. The figure displays three consecutive snapshots of the region in which the vortex solution with $m = 2$ shown in Fig. 3(c) takes sufficiently large values, namely, satisfying conditions $[\cos(\pi x)\cos(\pi y)]\,\mathrm{Re}\phi(x, y) > 0$ and $|\phi(x, y)| > 0.06$. The time interval between the snapshots is 1. This figure clearly shows that the vortex state indeed rotates with the frequency $\Omega \approx \mu/m$ in the OL potential. This figure also demonstrates that the vortex state with $m = 2$ is *stable*. The vortex solutions, with $m = 1$ and 2, to the asymptotic equation (5) are known to exist [18] and be dynamically stable [19] if N is smaller than a critical value. We have also checked the stability of the vortex states with $m = 1$ and 2, shown in Fig. 3, by direct numerical simulations of Eq. (2), starting from initial conditions in the form of perturbed vortex states. When the norm N is increased, more complicated behaviors are expected. Some simulation results such as a transition to a tightly bound state and a symmetry-breaking process are shown in the next section.

Solutions predicted by the asymptotic equation (5) near the BZ center,

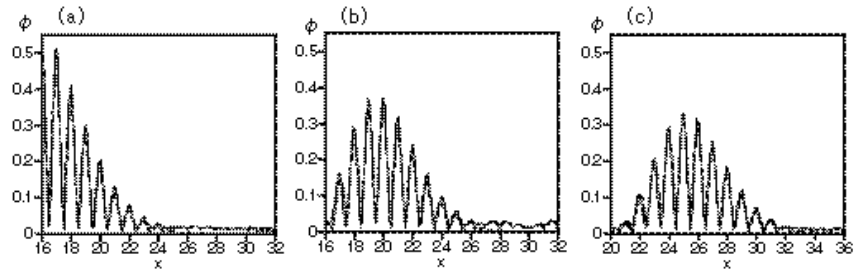

Figure 3: The central cross section of solutions $|\phi|$ for the loosely bound 2D states near the edge of the Brillouin zone with (a) $m = 0$, (b) $m = 1$, and (c) $m = 2$, which corresponds to Eq. (10). Solid and dashed curves depict, respectively, the solutions obtained from the asymptotic equation (5) and full GP equation (2).

i.e., corresponding to Eqs. (13) and (14), were also found, and compared to direct numerical solutions of the underlying GP equation (2). It should be stressed that, as the effective mass (14) is positive in this case, the corresponding localized solutions to the asymptotic equation (5) with $g > 0$ (repulsive interaction) are not soliton-like ones, but are instead close to the Thomas-Fermi (TF) states, that can be obtained neglecting the kinetic-energy term in the GP equation [14]. Figure 5 shows typical examples of thus found solutions for $m = 0$, $m = 1$, and $m = 2$. As is seen, the accuracy provided by Eqs. (5) and (13) is very good in this case, for all the values of m.

3.2 Relation to tightly bound solitons

The full GP equation (2) cannot be reduced to the asymptotic NLS equation (5) if the assumption of the slow variation of the envelope function is not valid; in that case, strongly confined ("tightly bound", TB) states may be possible, that are not described by Eq. (5). To investigate such solutions, and compare them to their loosely bound counterparts, we performed direct numerical integration of Eq. (2), looking for solutions that could be classified as having the vorticity $m = 0$ or $m = 1$ [in terms of Eq. (8)]. Figures 6(a)

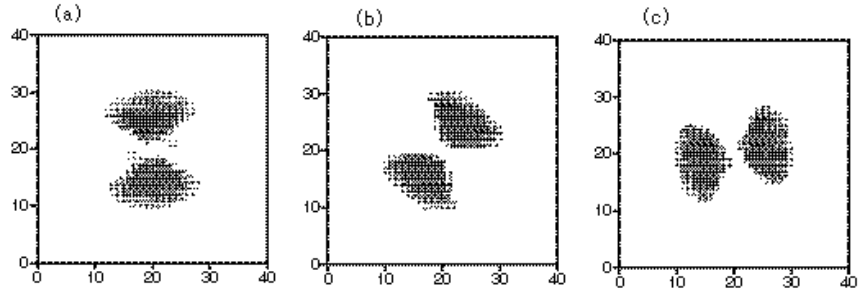

Figure 4: An example of the uniform rotation of the vortex state with $N = 4.08$ and $m = 2$.

and 6(b) display the amplitude of the thus found solutions [the maximum of $|\phi(x, y)|$] as a function of the norm, $N = \int\int |\phi|^2 dxdy$. The lower branches in these figures precisely correspond to the LB states described above, the dashed curves showing the dependence of the amplitude vs. N as found from the asymptotic equation (5). The solutions which belong to the upper branches in Fig. 6 can be identified as TB (strongly localized) 2D gap-soliton states in the GP equation with repulsive interaction between atoms, that persist in the limit of $B = 0$ and were first found in Refs. [4]. There is weak hysteresis for $m = 0$ between the LB and TB states for the parameter values of $\epsilon = 10$ and $B = -0.005$. The discontinuous transition between the LB and TB states occurs for sufficiently large ϵ. (The discontinuous transition was not observed for ϵ=5 and $B = -0.005$.) Figures 6(a) and (b) also make it obvious that the asymptotic equation (5) predicts a jump upward from the lower branch, which corresponds to the collapse in the asymptotic 2D NLS equation (5). However, the collapse does not occur in the full GP equation (2) with the repulsive nonlinearity (note that the negative effective mass is irrelevant when the localization length is on the same order of magnitude as the OL period). The critical value of the norm for the collapse in the asymptotic equation (5) is somewhat larger than the value at which the LB-TB transition occurs in the numerical solution of Eq. (2).

It is necessary to estimate the actual number of atoms in the BEC at which the LB-TB transition, shown in Fig. 6, is expected. Assuming a "pizza-shaped" condensate, with the diameter ~ 1000 OL periods and transverse width ten times smaller, taking the scattering length 5 nm (which is close to its value for ^{87} Rb), and following once again the derivation of the 2D equation

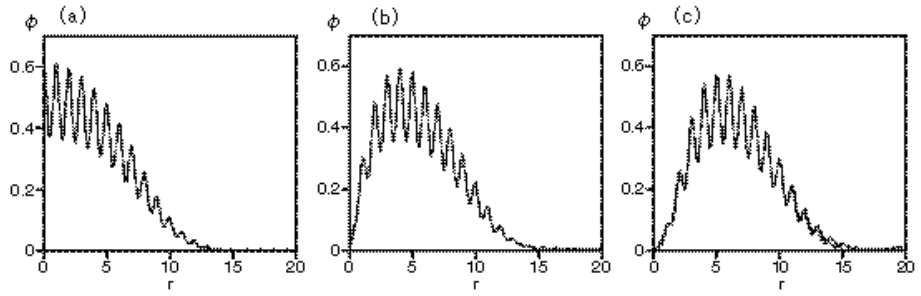

Figure 5: Dashed curves correspond to Thomas-Fermi-like solutions of the asymptotic equation (5) with $B = +0.005$ (the usual trap, rather than anti-trap) and positive effective mass, $M_{\rm eff} = 1.12$, as found by the shooting method from Eq. (9). These solutions describe loosely bound states close to the center of the Brillouin zone, as per Eq. (13). Continuous curves are numerical counterparts of these solutions, obtained from the full GP equation (2) with $\varepsilon = 5$. (a) $m = 0$, $N = 19.7$; (b) $m = 1$, $N = 29.8$; (c) $m = 2$, $N = 33.0$.

(2) from the full 3D GP equation, we conclude that the real number of atoms is obtained by multiplying the numbers on the horizontal axes in Fig. 6 by a factor $\simeq 10^3$.

To further illustrate the drastic difference between the LB and TB states with zero vorticity ($m = 0$), we display their typical examples, found as direct numerical solutions of Eq. (2), in Figs. 7(a) and (b). These figures display regions in which the absolute value of the respective solution exceeds the quarter-amplitude, i.e., $|\phi(x, y)| > |\phi|_{\max}/4$. Additionally, Fig. 7(c) displays the absolute value for both solutions, $|\phi(x, x)|$, as a function of x along the diagonal, $x = y$.

In a similar manner, the comparison of the LB and TB states with $m = 1$ is presented in Fig. 8, where the panels (a) and (b) again display regions where, respectively, the loose and tight solutions take the values with $|\phi(x, y)| > |\phi|_{\max}/4$, and the panel (c) shows the diagonal cross sections of both solutions. In particular, the TB vortex in Fig. 8(b) features a four-fold symmetry (it is invariant with respect to the rotation by $\pi/2$). In this connection, it is relevant to mention that, while the same symmetry is observed in all the TB vortices for a sufficiently large norm, $N \geq 10$, the four-fold symmetry is broken for $N \leq 9$.

To illustrate the latter property, Fig. 9 displays three consecutive snap-

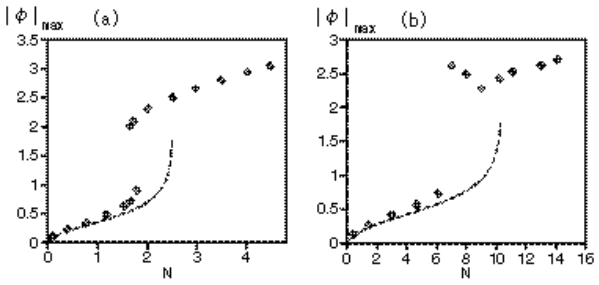

Figure 6: The amplitude of the 2D solution with $m = 0$ (a) and $m = 1$ (b) vs. the norm (number of atoms) N, in the case of $\varepsilon = 10$ and $B = -0.005$ [the dashed lines show the same dependencies, as predicted by the asymptotic equation (5) for the loosely bound states]. The lower and upper branches of the dependence correspond to the loosely and tightly bound states, respectively (see further details in the text).

shots of regions with $|\phi| > 0.5$, taken from the simulation starting with an LB vortex state that has $m = 1$ and $N = 7$. As is seen, the patterns do not feature the four-fold symmetry, unlike Fig. 8(b), but a nearly two-fold symmetric TB state is generated.

The transition between the less symmetric and more symmetric TB vortices accounts for the slope breaking in the amplitude-vs.-norm curve for $N = 9$, which is evident in Fig. 6(b). We have also found the TB vortices with $m = 2$ and checked that they are stable as well. Figure 10 displays the TB vortices with $m = 2$ for $N = 3.92$ and $N = 48.1$. Figures 10(a) and (b) display the regions where the TB solutions take the values with $|\phi(x, y)| > |\phi|_{\max}/4$, and the panel (c) shows the cross sections along the line $y - L/2 = -0.45(x - L/2)$, on which $|\phi|$ takes the maximum value for $N = 48.1$. To the best of our knowledge, the existence of TB vortex solitons in the 2D model with self-repulsion has not been reported before, therefore theses result (displayed here for $m = 1$ and 2) are novel by themselves too (similar stable vortices were very recently found by means of a different method [20]).

The localized solutions belonging to the LB and TB branches differ dras-

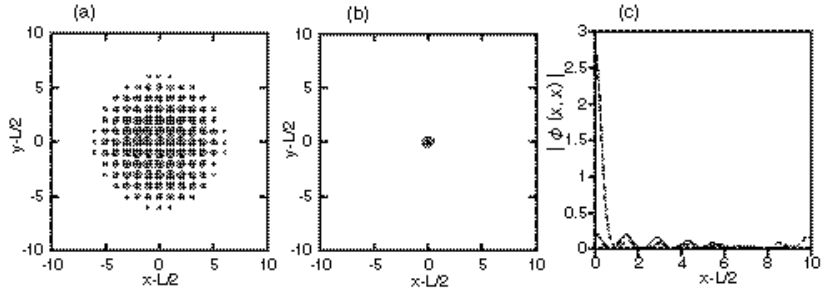

Figure 7: Typical examples of the loosely (a) and tightly (b) bound 2D states with $m = 0$ (zero vorticity) for $\varepsilon = 10$ and $B = -0.005$. The norms of the two states are, respectively, $N_{\rm loose} = 0.393$ and $N_{\rm tight} = 2.66$. Panel (c) displays the diagonal cross sections of the two solutions, $|\phi(x, x)|$ (the solid and dashed lines depict the loosely and tightly bound states, respectively).

tically not only in the dependence of $|\phi|_{\max}$ vs. N (i.e., in their static properties), but in dynamical properties too. As it will be shown in the next section, the TB solitons are always pinned by the underlying OL potential, while the LB states may move freely. In fact, a sharp transition between mobile and immobile 1D solitons with $M_{\rm eff} < 0$ (i.e., close to the BZ edge) and $g > 0$ (repulsive interactions) was reported in Ref. [13]. As well as in the 2D case, the immobilization takes place with the increase of the soliton's norm, and no hysteresis between the mobile and immobile solitons is found.

The abrupt transition between the LB and TB localized states, as described above, is a characteristic feature of the localized states with the negative effective mass, found close to the BZ edge, where the LB state is well approximated by Eqs. (4), (8), and (10). On the other hand, no similar transition is found for the localized states close to the BZ center, where the approximation (10) is replaced by (13). The absence of the distinction between LB and TB states in the latter case is explained by the fact that, as is commonly known, TB solitons simply do not exist in the case of the

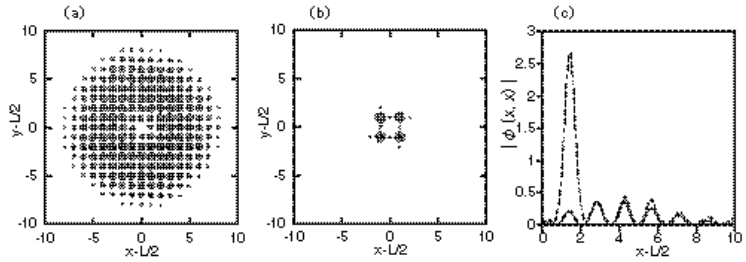

Figure 8: The same as in Fig. 7 for the loosely (a) and tightly (b) bound vortices with $m = 1$. The norms of the two states are, respectively, $N_{\rm loose} = 0.413$ and $N_{\rm tight} = 13$.

self-repulsion ($g > 0$) near the BZ center. Localized LB states of course exist, as suggested by the TF approximation.

4 Motion of loosely bound localized states

In the 2D model with both repulsive [4] and attractive [6] interaction, the TB solitons are strongly pinned by the OL potential, and cannot move (stable TB solitons also exist in the 2D attractive model with a quasi-1D periodic

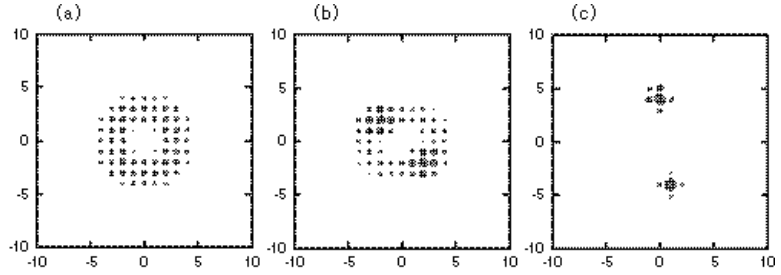

Figure 9: Three snapshot patterns taken at the moments (a) $t = 10$, (b) $t = 40$, and (c) $t = 80$ in the simulation of a loosely-bound vortex with $m = 1$, evolving into a tightly-bound state. The norm is $N = 7$.

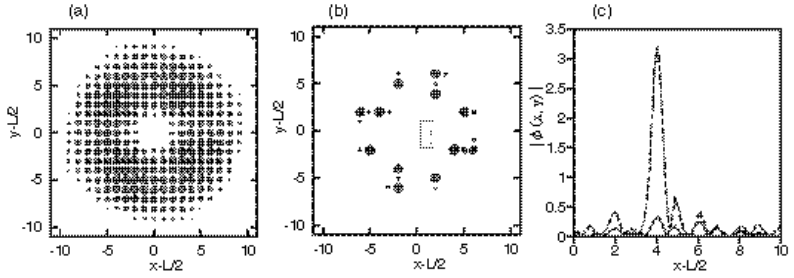

Figure 10: The same as in Figs. 7 and 8 for the loosely (a) and tightly (b) bound vortices with $m = 2$. The norms of the two states are, respectively, $N_{\rm loose} = 3.92$ and $N_{\rm tight} = 48.1$. (c) A profile of $|\phi(x, y)|$ for the tightly-bound vortex along the line $y - L/2 = -0.45(x - L/2)$.

potential, and in the 3D model with a quasi-2D potential, in which case they may freely move in the unconfined direction [20]). On the contrary to that, the LB localized states described above may move freely on top of the underlying 2D periodic potential, keeping their coherent structure. This feature resembles a similar one that we have recently demonstrated in the 1D version of the present model [13]; in particular, the 1D solitons with the negative effective mass are expelled by the ordinary parabolic trap, and are held by the anti-trap. However, the character of the motion in the 2D case may be completely different, see below.

A 2D LB state can be set in motion either by an initial shift from the central position [relative to the (anti-)trap], or by lending it an initial momentum. We have performed numerical simulations, using both ways to push the localized state. For instance, Fig. 10 displays results obtained with the initial condition $\phi(x, y, 0) = \phi_0(x-5, y) \exp(ikq_y y)$, where $\phi_0(x, y)$ is the stationary LB state with $m = 0$ and $N = 0.479$, whose peak position is located at the central point, $(L/2, L/2)$, and $q_y = 0.2$. In other words, this initial condition implies that the localized state is pushed by shifting its center in the x direction, and giving it an initial momentum along y.

We define the instantaneous position of the center of the localized state as $\mathbf{X} = \int\int \mathbf{x}|\phi(x, y; t)|^2 dxdy / \int\int |\phi|^2 dxdy$. Figure 11(a) demonstrates that, as a result, the center of the LB state moves along an elliptic trajectory [in the case

displayed in Fig. 11(a), the simulations were run up to the time $t_{\max} = 100$, while the numerically measured period of the elliptic motion was $T_{\rm num} \approx 88$, i.e., the localized state has completed one full circulation (in the clockwise direction, since the initial velocity $v_y = q_y/M_{\rm eff}$ is negative). To make the difference from the strongly pinned TB solitons clearer, Fig. 11(b) displays a result of a similar attempt to set in motion the localized state of the TB type. As a result, initially its center moves irregularly, and is then trapped by the OL potential. Many other runs of the simulations produced quite similar results; in particular, the eccentricity of the elliptic orbit depends on the initial push, and effectively 1D periodic motion along straight lines through the center of the domain are possible too. In this connection, it is relevant to mention that, although the underlying OL makes the medium anisotropic, simulations do not reveal any dependence of the frequency on the direction of the 1D oscillations (the frequency of the elliptic motion does not depend on the orientation of the ellipse either).

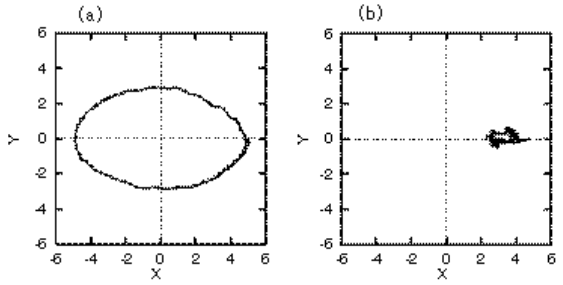

Figure 11: Panel (a) displays a typical example of the stable elliptic motion of a localized loosely-bound state with zero vorticity ($m = 0$) and negative effective mass ($M_{\rm eff} \approx -1.03$) in the *anti-trap* with $B = -0.005$. In this case, $\varepsilon = 10$, and the norm of the localized state is $N = 0.479$. For comparison, panel (b) displays an attempt to set in motion a tightly-bound soliton with $N = 4.01$.

The periodic motion of the LB state can be easily described within the framework of the asymptotic equation (5). In that case, one can demonstrate that motion for the center $\mathbf{X}$ of the localized state, which is treated as a rigid

quasi-particle, obeys the Newton's equation of motion,

$$M_{\rm eff}\frac{d^2\mathbf{X}}{dt^2} = -B\mathbf{X} \tag{16}$$

[$M_{\rm eff}$ is the same effective mass as in Eq. (5), while the right-hand side is the potential force generated by the parabolic (anti-)trap]. Equation (16) indeed describes the observed motion with a good accuracy. For instance, in the case displayed in Fig. 8 (a), Eq. (16) predicts the period of the motion,

$$T_{\rm anal} = 2\pi\sqrt{M_{\rm eff}/B} \approx 90, \tag{17}$$

which should be compared to the above-mentioned numerically found period, $T_{\rm num} \approx 88$.

As it was explained above, the localized states found close to the BZ center are actually always of the LB type, hence one may expect that they may move freely too. This is indeed observed in simulations. Typical examples are displayed in Fig. 12, for the localized states with $m = 0$ and 2 (quite a similar motion mode was observed for the vortex with $m = 1$). The trajectory corresponds to anti-clockwise elliptic circulation in this case, as the initial velocity $v_y = q_y/M_{\rm eff}$ is positive.

We stress that the vortex LB states readily exhibit circular motion with the same period as their counterparts with $m = 0$, and the analytical prediction for the circulation period, based on Eq. (17), is very accurate in this case too. For example, in both cases ($m = 0$ and $m = 2$) shown in Fig. 12, the predicted period is $T_{\rm anal} \approx 94.0$, while the one extracted from the numerical data is $T_{\rm num} \approx 94.5$.

5 Conclusion

In this work, we have developed analysis of dynamics of nonlinear localized excitations in two-dimensional (2D) Bose-Einstein condensates (BECs) with repulsive interactions, which are subjected to the action of the optical lattice (OL) combined with the external parabolic potential. First, we have shown, in an analytical form, that broad ("loosely bound", LB) localized states, based on the 2D Bloch function near the edge of the Brillouin zone (BZ), feature a negative effective mass (while the mass of the LB localized states is positive near the BZ center). The negative-mass pulse cannot be confined by

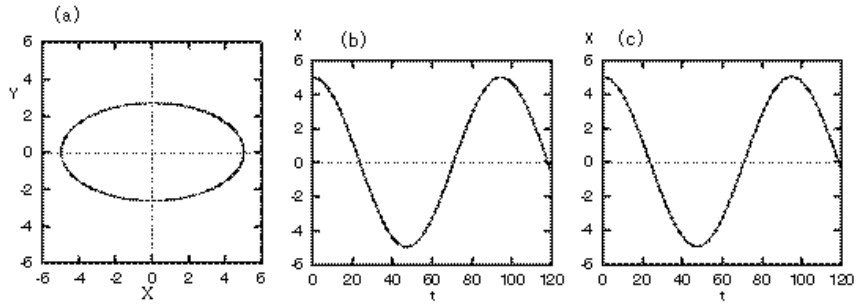

Figure 12: Panel (a) has the same meaning as in Fig. 11, but for the case of the positive effective mass, $M_{\text{eff}} \approx 1.12$, and in the ordinary trap with $B = +0.005$ (and $\varepsilon = 5$). Panel (b) shows the corresponding time dependence of the central coordinate X of the moving localized state. In panel (c), the same dependence is shown for the circular motion of the vortex with $m = 2$.

the usual trap, but it is held by an inverted parabolic potential (*anti-trap*). Direct simulations have demonstrated that the LB states (including vortices) are stable and can freely move on top of the OL, and the frequency of their periodic motion along an elliptic orbit in the anti-trapping potential agrees very well with the analytical prediction, which treats the LB solitons as quasi-particles. Besides that, the LB vortices feature rotation around the center. With the increase of the number of atoms, an abrupt transition occurs, from the negative-mass LB states to their tightly bound (TB) counterparts; unlike the LB states, the TB solitons are rigidly pinned by the OL. The positive-mass LB states (including vortices), constructed near the BZ center, are stable and move freely too.

Further dynamical effects may be considered in the 2D situation, such as collisions between moving solitons. In fact, various types of collisions are possible, such as between zero-vorticity solitons and vortices, as well as between LB and TB states with the negative mass (the latter is possible in the presence of the anti-trap). On the other hand, interactions between solitons with positive and negative mass are precluded, as only one type of the solitons may be confined by a given trapping or anti-trapping potential. The consideration of collisions is, however, beyond the scope of this paper.

We expect that similar LB and TB states may be found in BECs subject to the action of the 3D (three-dimensional) OL potential. However, simulations of the corresponding 3D GP equation is a rather difficult problem.

Estimates for physical parameters at which the predicted effects may be observed are similar to those in the 1D counterpart of the model [13] . In particular, a circular motion of the LB soliton in the anti-trap may be expected at a frequency ~ 100 Hz in a domain of the diameter ~ 0.5 mm ($\simeq 1000$ spatial periods of the OL). The transition from the LB to TB solitons is expected when the number of atoms in the condensate attains the values between $\simeq 2 \cdot 10^3$ for the $m = 0$ states and $\simeq 6 \cdot 10^3$ for the vortex with $m = 1$.

In the experiment, the LB and TB localized states are expected to form spontaneously from a properly chosen number of atoms loaded in the appropriate potential, as there is virtually no overlap between these two types of the states. As concerns vortex states, they may be created using the well-known technique of optical stirring. The effects predicted in this work for the BEC can also take place with spatial optical solitons in bulk photonic crystals.

Acknowledgements

The work of B.A.M. was supported, in a part, by the Israel Science Foundation through a grant No. 8006/03.

References

References

[1] Greiner M, Bloch I, Mandel O, Hansch T W, and Esslinger T, Appl. Phys. 2001 B **73**, 769; Han D J, DePue M T, and Weiss D S 2001 Phys. Rev. A **63** , 023405; Greiner M, Mandel O, Hansch T W, and Bloch I 2002 Nature **419**, 51; Mellish A S, Duffy G, McKenzie C, Geursen R, and Wilson A C 2003 Phys. Rev. A 68, 051601; Bloch I, Greiner M, Mandel O, and Hansch T W 2003 Phil. Trans. Roy. Soc. L., Ser. A **361**, 1409.

[2] Khaykovich L, Schreck F, Ferrari G, Bourdel T, Cubizolles J, Carr L D, Castin Y and Salomon C 2002 Science **296**, 1290; Strecker K E, Partridge G B, Truscott A G and Hulet R G 2002 Nature **417** 150; 2003 New J. Phys. **5** 73.

[3] Anker Th, Albiez M, Eiermann B, Taglieber M, and Oberthaler M K 2004 e-print cond-mat/0401165.

[4] Baizakov B B, Konotop V V and Salerno M 2002 J. Phys. B **35** 5105.

[5] Konotop V V and Salerno M 2002 Phys. Rev. A **65** 021602; Louis P J Y, Ostrovskaya E A, Savage C M, and Kivshar Y S 2003 Phys. Rev. A **67** 013602; Ostrovskaya E A and Kivshar Y S 2003 Phys. Rev. Lett. **90** 160407.

[6] Baizakov B B, Malomed B A, and Salerno M 2003 Europhys. Lett. **63** 642.

[7] Yang J and Musslimani Z H 2003 Opt. Lett. **28** 2094.

[8] Carusotto I, Embriaco D and La Rocca G C 2002 Phys. Rev. A **65** 053611; Hilligsoe K M, Oberthaler M K and Marzlin K P 2002 *ibid.* A **66** 063605; Kevrekidis P G, Frantzeskakis D J, Malomed B A, Bishop A R and Kevrekidis I G 2003 New J. Phys. **5** 64; Scott R G, Martin A M, Fromhold T M, Bujkiewicz S, Sheard F W, and Leadbeater M 2003 Phys. Rev. Lett. **90** 110404; Efremidis N K and Christodoulides D N 2003 Phys. Rev. A **67** 063608.

[9] Xi P, Zhang Z-Q and Zhang X 2003 Phys. Rev. E **67** 026607.

[10] Malomed B A, Wang Z H, Chu P L, and Peng G D 1999 J. Opt. Soc. Am. B **16** 1197.

[11] Fleischer J W, Segev M, Efremidis N K, and Christodoulides D N 2003 Nature **422**, 147.

[12] Jeng C C, Shih M F, Motzek K, and Kivshar Y 2004 Phys. Rev. Lett. **92**, 043904; Fleischer J W, Bartal G, Cohen O, Manela O, Segev M, Hudock J, and Christodoulides D N 2004 Phys. Rev. Lett. **92**, 123904.

[13] Sakaguchi H and Malomed B A 2004 J. Phys. B: At. Mol. Opt. Phys. **37**, 1443.

[14] Dalfovo F, Giorgini S, Pitaevskii L P and Stringari S 1999 Rev. Mod. Phys. **71**, 463.

[15] Band Y B, Towers I, and Malomed B A 2003 Phys. Rev. A **67**, 023602.

[16] Ruprecht R A, Holland M J, Burnett K, and Edwards M 1995 Phys. Rev. A **51**, 4704.

[17] Ueda M and Leggett A J 1998 Phys. Rev. Lett. **80**, 1576.

[18] Dalfovo F and Stringari S 1996 Phys. Rev. A **53**, 2477.

[19] Saito H and Ueda M 2002 Phys. Rev. Lett. **89**, 190402.

[20] Baizakov B B, Malomed B A, and Salerno M 2004, to be published.